Rapid Communications

Room-temperature polar metal stabilized under high pressure

J.-J. Gao,[1,2] S.-Y. Fu,[3] K. Yamaura,[4,5] J. F. Lin,[3] and J.-S. Zhou[1,*]

[1]*Materials Science and Engineering Program, Mechanical Engineering, The University of Texas at Austin, Austin, Texas 78712, USA*

[2]*Institute of Fluid Physics, China Academy of Engineering Physics, Mianyang 621900, China*

[3]*Department of Geological Sciences, The University of Texas at Austin, Austin, Texas 78712, USA*

[4]*International Center for Materials Nanoarchitectronics (WPI-MANA), National Institute for Materials Science, 1-1 Namiki, Tsukuba, Ibaraki 305-0044, Japan*

[5]*Graduate School of Chemical Sciences and Engineering, Hokkaido University, North 10 West 8, Kita-ku, Sapporo, Hokkaido 060-0810, Japan*

(Received 24 January 2020; accepted 15 May 2020; published 2 June 2020)

$LiOsO_3$ synthesized under high pressure in recent years is a rare metal since it undergoes a nonpolar to polar phase transition at $T_s = 140$ K. Forming a polar axis through a phase transition in a metal seems against common sense. It is also not clear whether the transition to a polar phase in the oxide fits the mechanism predicted by Anderson and Blount in 1965. As monitored by an anomaly of resistivity in $LiOsO_3$ at T_s reported recently, T_s increases under pressure. The structural study under high pressure could give us a useful clue for understanding how dipoles form in this metallic oxide. Here, we report the identification of a polar phase of $LiOsO_3$ at room temperature under high pressure by using *in situ* probes of Raman and synchrotron x-ray diffraction. In the Raman study, the pressure-induced modes and their responses to polarized light, the linewidth change, the peak profile change, and mode softening have been directly compared with the corresponding changes of $LiOsO_3$ on cooling through T_s at ambient pressure. Whereas a complete set of Raman modes from the $R3c$ phase can be found at $P \geqslant 15.5$ GPa, a Raman mode of the $R3c$ phase appears in the $R\bar{3}c$ phase at 4.11 GPa. A significant drop in the linewidth occurs at 12.6 GPa that coincides with the critical pressure for the phase transition to the polar phase detected by x-ray diffraction. Fitting the peak profile of a Raman mode to the Fano formula also indicates a clear change of electron-phonon coupling at 16 GPa. In contrast to a sharp structural transition to the polar phase at T_s under ambient pressure, our results reveal all the structural ingredients to facilitate the polar phase over a broad range of pressure. A bond valence sum analysis has been introduced to reveal the local structural instability under pressure. The transition to the polar phase in metallic $LiOsO_3$ is solely caused by optimizing the local structure in order to make the bond valence sum close to the formal valence of the Li ion.

DOI: 10.1103/PhysRevB.101.220101

Almost all ferroelectric materials are insulators. In a metal, free electrons screen the long-range Coulomb interactions to prevent the formation of ferroelectricity. Anderson and Blount [1] postulated the possibility of forming a "ferroelectric" metal through a second-order phase transition where a polar axis can be formed. The key idea is that free electrons in a compound do not interact very strongly with transverse optical (TO) phonons, and the Lorentz local fields lead to "ferroelectricity." The synthesis of $LiOsO_3$ in recent years [2] has revived interest in the idea of a "ferroelectric" metal. By using ultrafast spectroscopy, Laurita *et al.* [3] provided evidence of a weak electron-TO phonon (WETP) coupling in $LiOsO_3$. However, it is still unclear whether the WETP leads to a polar transition or if it is a consequence of the transition. Recent developments on understanding the mechanism of a polar transition in a metal indicate that polar instabilities are driven by optimizing the local bonding environment [4,5] specifically, the Li ion bonding with out-of-plane oxygen atoms to form the LiO_6 octahedra in $LiOsO_3$ [6,7]. Gu *et al.* [8] have shown recently a correlation between a ferroelectric displacement and an octahedral-site rotation (OR), which rationalizes ferroelectricity in the oxides with a $LiNbO_3$ (LNO) structure. Verification of these ideas is critically important for the design of new polar metals. In this Rapid Communication, we report that the transition temperature to the polar phase of $LiOsO_3$ can reach to room temperature at 16 GPa. More importantly, our study reveals in detail all the structural ingredients to facilitate the polar displacement in the metallic $LiOsO_3$.

Detailed information on the Raman experiment, synchrotron x-ray diffraction with a diamond anvil cell (DAC), results of Rietveld refinement, and the equation of state are provided in the Supplemental Material (SM) [9]. Raman spectra from sample No. 1 at several pressures are shown in Fig. 1(a); the Raman spectra at all pressures are shown in Fig. S1, together with results on the other three samples. The Raman spectra are highly repeatable. At $P = 0.44$ GPa, the observed four Raman-active modes labeled ^1E_g, ^2E_g, ^3E_g, and ^4E_g match perfectly those at room temperature and ambient pressure reported in the literature [10]. At $P \geqslant 4.11$ GPa, a shoulder appears at the higher-energy side of the ^2E_g peak. By taking advantage of single-crystal samples, a polarization analysis of the spectrum helps to determine the symmetry of

*jszhou@mail.utexas.edu

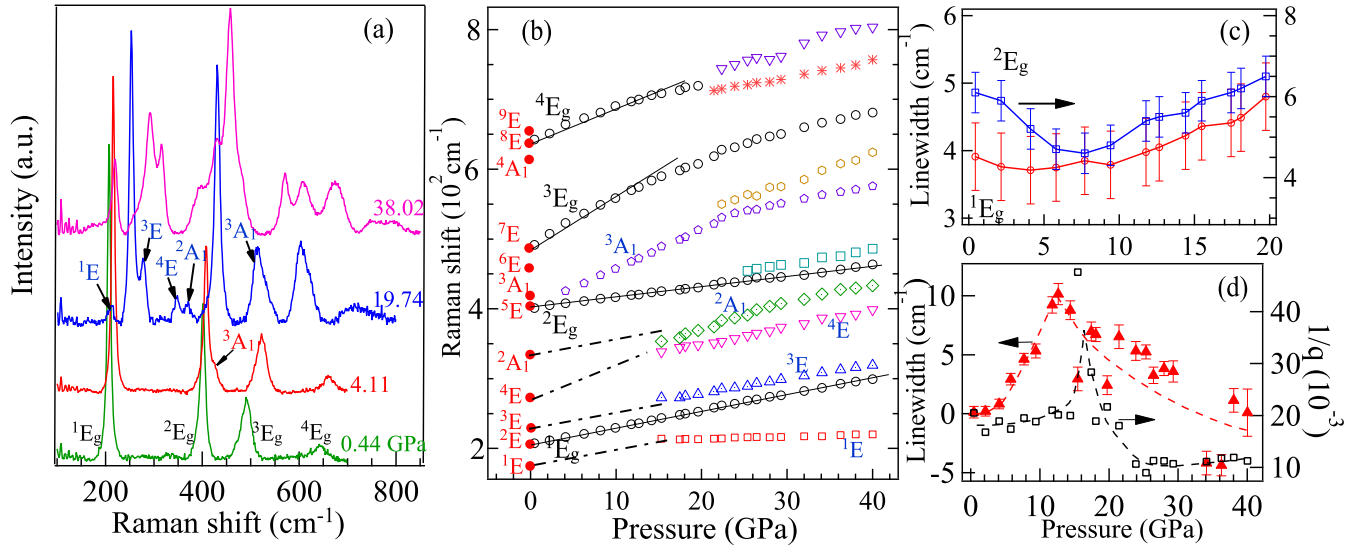

FIG. 1. (a) Room-temperature Raman spectra at several pressures; (b) the pressure dependence of Raman modes in $LiOsO_3$; solid symbols for the $R3c$ phase at ambient pressure are after Ref. [10]; (c) the pressure dependence of linewidth for ^1E_g and ^2E_g in the $R\bar{3}c$ phase; (d) the pressure dependence of linewidth and the asymmetric factor for ^3E_g on crossing the phase transition from $R\bar{3}c$ to $R3c$. Error bars are smaller than symbols if not specified.

the phonon modes involved as shown in Fig. S2; this character matches precisely that of the $^3A_1$ mode of the polarized-light Raman spectrum in the polar phase below T_s at ambient pressure [10]. By using the same procedure, we can uniquely identify the peaks shown in the spectrum at 19.74 GPa in Fig. 1(a); these peaks can be assigned to ^1E, ^3E, ^4E, and $^2A_1$. The onset pressure for these peaks is as low as 15.48 GPa in Fig. S2. The intensity of the Raman scattering becomes weak through a DAC, which makes it difficult to discern weak peaks in spectra above 600 cm^{-1}. Nevertheless, at $P \geqslant 15.48$GPa, the number of Raman peaks below 600 cm^{-1} and how the peak intensity changes in responding to the polarized light match perfectly the modes in the polar phase at ambient pressure.

Lattice vibrations are strengthened under high pressure in a solid [11]. In the nonpolar phase of $LiOsO_3$, although $d\upsilon/dP > 0$ can be found for all four Raman peaks in Fig. 1(b), where υ is the mode frequency, the magnitude of $d\upsilon/dP$ for ^1E_g and ^2E_g is sharply lower than that for ^3E_g and ^4E_g. The mode-Grüneisen parameters γ calculated from the $d\upsilon/dP$ and the bulk modulus for the nonpolar phase of $LiOsO_3$ are 2.01 (^1E_g), 0.65 (^2E_g), 2.42 (^3E_g), and 1.3 (^4E_g) which are comparable to that of $La_xSr_{2-x}MnO_4$ [12]. Relative to the mode frequencies in the $R3c$ phase below T_s at ambient pressure, the pressure-induced modes of the polar phase at $P \geqslant 15.48$GPa must have higher frequencies. On the assumption that the $d\upsilon/dP$ for ^1E, ^3E, and $^2A_1$ is close to that for ^1E_g, the onset frequency of ^1E, ^3E, and $^2A_1$ at 15.48 GPa can be closely projected by the dashed lines in Fig. 2(b). The same is true for the ^4E mode based on the $d\upsilon/dP$ of ^4E_g. From both the polarization analysis and the pressure dependence of frequency for these modes appearing at $P > 15.48$GPa, the high-pressure phase of $LiOsO_3$ is identical to the polar structure below T_s at ambient pressure.

Vibrations in $LiOsO_3$ with the LNO structure include the relative motions between the Li and OsO_6 octahedron and internal motions of the OsO_6 octahedron. The four A_1 modes in the structure become Raman and IR active only with the site symmetry C_{3v} [10]. The $^3A_1$ mode refers to the octahedral rotation around the c axis of the rhombohedral cell [10]. The $^3A_1$ mode appearing at $P = 4.11$ GPa implies that the local site symmetry is reduced to the C_{3v} in a matrix of the $R\bar{3}c$ phase. A larger $d\upsilon/dP$ in the $LiOsO_3$ crystal is obtained for the vibrational modes associated with either changing of the Os-O bond length or the rigid rotation of OsO_6 octahedra, i.e., ^3E_g, ^4E_g, and $^3A_1$ modes. In the Raman study at ambient pressure, all $^{1-4}E_g$ modes continue on crossing the nonpolar to polar phase transition and show a mode softening at T_s [10]. Based on the extrapolation of the ordinary temperature-dependent phonon frequency in the nonpolar phase to the lowest temperature, a frequency reduction $\Delta\upsilon/\upsilon = -0.012$ for ^1E_g, -0.005 for ^2E_g, and -0.022 for ^3E_g is obtained due to the transition to the polar phase at ambient pressure. As shown in Fig. 1(b), the pressure-induced mode strengthening has a rate $\Delta\upsilon/\upsilon \sim 0.5$ over 40 GPa for the $^{1-2}E_g$ modes. The mode softening at a critical pressure for these two modes must be negligible in comparing with the overwhelming mode strengthening under pressure. The ^3E_g mode shows an obvious softening at T_s. The mode is also most sensitive to pressure at $P < 15$GPa and exhibits obvious softening for $P > 15$GPa; which is consistent with the pressure-induced transition to the polar phase.

Since multiple peaks develop near positions of ^1E_g and ^2E_g for $P > 20$ GPa, fitting the peak to the Fano formula has been only done up to 20 GPa for these two modes and the result is displayed in Fig. 1(c). The linewidth reduction of the ^1E_g and ^2E_g modes upon increasing pressure resembles the linewidth reduction as temperature decreases in the $R\bar{3}c$ phase at ambient pressure [10]. However, the effect of non-hydrostaticity in the pressure medium normally broadens the linewidth in a high-pressure Raman study [11]. In our case, the pressure medium neon becomes a solid at 4.7 GPa [13]

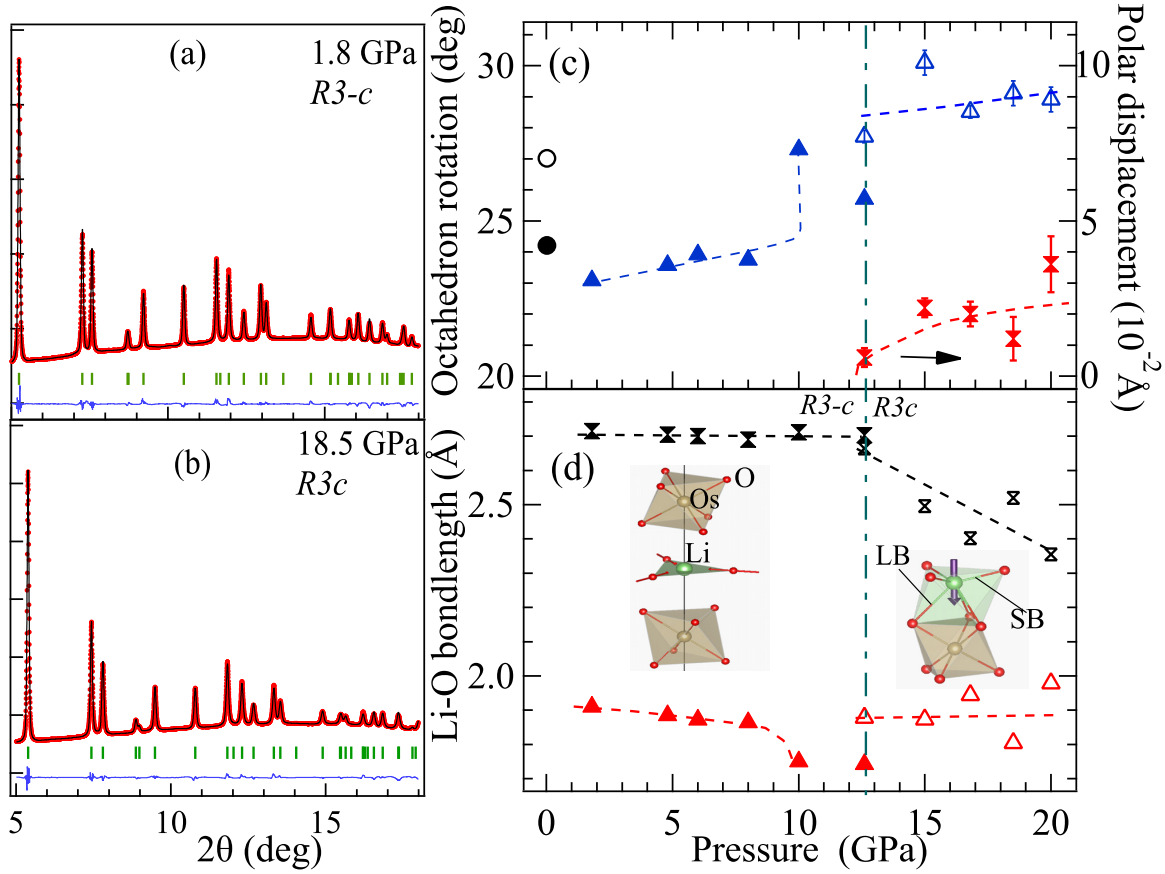

FIG. 2. (a), (b) Room-temperature synchrotron x-ray diffraction patterns of $LiOsO_3$ at 1.8 and 18.5 GPa and results of Rietveld refinement. (c) Pressure dependences of the rotation angle of the OsO_6 octahedron and the Li displacement and (d) the Li-O bond length in the LiO_x polyhedron in $LiOsO_3$. Error bars are smaller than symbols if not specified. Dashed lines are a guide to the eyes. Inset: The structural models of atoms surrounding Li in the $R\bar{3}c$ and $R3c$ phases. Arrows point to the direction of shifting the oxygen position in the $R\bar{3}c$ model and shifting the Li position in the $R3c$ model under high pressure.

and it is reasonable to attribute the linewidth broadening at $P > 5$ GPa.

The ^3E_g mode is the in-plane vibration of the Li ion relative to the OsO_6 octahedra, which is coupled to the out-of-plane, IR-active mode A_{2u} of Li vibration along the direction of polar displacement [10]. As the A_{2u} mode softens, the Li moves into a LiO_6 octahedron. The change of local bonding environment is reflected in the most dramatic change in both mode frequency and the linewidth of the ^3E_g mode as seen from the Raman study at ambient pressure [14]. In order to get detailed information on the linewidth change of the ^3E_g mode under pressure, we fit the normalized linewidth change of the ^1E_g mode under pressure to a polynomial function and subtract it from the raw data of the ^3E_g linewidth versus pressure; see Fig. S3 for details. Figure 1(d) displays the background-corrected linewidth of the ^3E_g mode versus pressure; the linewidth increases with pressure and exhibits an abrupt drop at $P \approx 12.6$ GPa, which is stunningly similar to the linewidth change on cooling through T_s at ambient pressure [14]. The linewidth drop at 12.6 GPa implies a pressure-induced disorder-order transition similar to the change at T_s. The critical pressure 12.6 GPa from Fig. 1(d) coincides with the pressure for a phase transition detected by x-ray diffraction as discussed below. Fitting the peak profile of the ^3E_g mode to the Fano formula also gives the asymmetry factor $|1/q|$, which is an indicator of electron-phonon coupling. The pressure dependence of $|1/q|$ in Fig. 1(d) resembles a λ shape in contrast to a steplike change on cooling through T_s. The electron-phonon coupling becomes sharply weak in the polar phase as seen from a reduced $|1/q|$. It should be noted that the $|1/q|$ peaks out at $P \approx 16$ GPa where all Raman modes of the $R3c$ phase appear. The tail of $|1/q|$ on the high-pressure side goes well into the pressure range for the polar phase. This result implies a much-enhanced electron-phonon coupling in the $R\bar{3}c$ phase near the boundary to the $R3c$ phase. A weak electron-phonon coupling is the consequence of the phase transition to the $R3c$ phase, not a driving force.

Figures 2(a) and 2(b) display synchrotron x-ray diffraction patterns collected under 1.8 and 18.5 GPa and the refinement results with $R\bar{3}c$ and $R3c$ structural models, respectively. The patterns under all pressure points in Fig. S5 look similar and can be refined reasonably well with either the $R\bar{3}c$ or the $R3c$ phases. The reliable factors R_p and χ^2 are useful to determine if x-ray diffraction can indeed be helpful to distinguish these two structures. As displayed in Fig. S6, the overall fitting reliability is good below 21 GPa. The shearing stress causes much-enhanced R_p and χ^2 at $P > 21$ GPa. The following structural analysis is limited at $P \leqslant 21$ GPa. Both R_p and χ^2 from the refinement with the $R\bar{3}c$ model are consistently smaller below $P \leqslant 12.66$ GPa, whereas they are

consistently smaller for the refinement with the $R3c$ model at $P \geqslant 12.66$ GPa. This observation confirms the phase transition to the polar phase at $P = 12.66$ GPa. At 12.66 GPa, refinements with both models yield the identical R_p and χ^2. The determination of the crystal structure at this pressure point relies on the analysis of the bond valence sum (BVS) discussed below.

For the $R\bar{3}c$ phase, the angle ω of OR can be calculated through the formula $\tan\omega = \sqrt{3}-x\sqrt{12}$ [15], where x is the oxygen position $(x, 0, 0.25)$. For the polar $R3c$ phase, the oxygen is at $(1/6-u, 1/3+\upsilon, 1/12)$ and ω is calculated through the formula $\omega = u/(\sqrt{3}/16)$ [16]. From the data at ambient pressure [2], the OR jumps from $\omega = 24.21^\circ$ to 27.04° on crossing the transition from the $R\bar{3}c$ to the $R3c$ phase on an assumption that the temperature dependence of ω is negligible. As shown in Fig. 2(c), ω obtained at $P = 0.44$ GPa is close to the value at ambient pressure; it increases slightly with pressure to 8 GPa, followed by a jump to $\omega = 27.3^\circ$ at 10 GPa. It is important to know that while $LiOsO_3$ is still in the $R\bar{3}c$ phase, the OR becomes as large as that in the $R3c$ phase. From the BVS analysis below, an increased OR and the consequent bond length change are the precursor for the pressure-induced phase transition to the polar phase. At $P = 12.6$ GPa, the refinement with the $R\bar{3}c$ and the $R3c$ phases gives different OR values. The Li polar displacement can be obtained from the refinement with the $R3c$ phase at 12.6 GPa and the displacement increases monotonically as pressure increases further. The Li displacement appears to correlate with the increase of the OR.

Li in the $R\bar{3}c$ phase of $LiOsO_3$ locates in the triangle plane with oxygen atoms as illustrated in the inset of Fig. 2(d); Li forms three short bonds (SBs) to oxygen in the triangle plane and six long bonds (LBs) to oxygen on the two neighboring OsO_6 octahedra. The calculation by Benedek and Birol (BB) indicates that the SB decreases while the LB increases as the OR increases for both the $R\bar{3}c$ and $R3c$ phases [6]. Due to the Li polar displacement, the $R3c$ phase has a longer SB and shorter LB than those in the $R\bar{3}c$ phase at a given OR. The authors have argued that the $R3c$ phase is stabilized by the consideration of the bond valence. The local structure can be tuned with pressure in this picture, which could help to identify the driving force for the polar transition. The SB, the LB and, the OR $\omega = 23^\circ$ of $LiOsO_3$ at $P = 1.8$ GPa in Fig. 2(d) are extremely close to those at ambient pressure calculated by BB. Corresponding to the pressure-induced increase of OR in the $R\bar{3}c$ phase, the SB changes in a rate $\Delta SB/\Delta\omega \approx -0.5$ (Å/deg) [estimated from the dashed lines in Figs. 2(c) and 2(d)]; a similar rate is obtained for the jump of $\Delta\omega$ and the associated drop of ΔSB from 8 to10 GPa. In contrast, the calculation by BB gives a $\Delta SB/\Delta\omega \approx -0.029$ (Å/deg). From the geometry of the LNO structure, the SB reduces as the OR increases. Under the circumstance of applying high pressure, the SB is subjected to a uniform reduction on top of the reduction due to an increased OR, which is the origin for a larger $\Delta SB/\Delta\omega$ under high pressure. The pressure-induced reduction of the LB must compensate the increase of the LB due to the change of OR, so that the LB remains pressure independent in the $R\bar{3}c$ phase. On the side of the $R3c$ phase in Figs. 2(c) and 2(d), while the OR increases slightly with pressure, the SB is nearly pressure independent. A dramatic reduction of the LB in the $R3c$ phase indicates that the pressure effect is to move the Li toward the center of the LiO_6 octahedron. These pressure-induced local structural changes on both sides of the phase boundary must convey useful information leading to the driving force for the phase transition.

Since the band structural calculations show that electrons at the Fermi energy are primarily from the Os : $5d$ and O : $2p$ bands in the OsO_6 octahedra [7,17], the localized electron picture such as the bond valence sum (BVS) could be a suitable parameter to describe the structural stability in Li-O polyhedra. As a test to this thought, we calculated the BVS of Li in the Li-O polyhedra for both $R\bar{3}c$ and $R3c$ phases at ambient pressure; it is 1.195 for $R\bar{3}c$ and 1.166 for $R3c$, which are very close to the formal valence of the Li ion. The difference between the BVS and the formal valence provides a measurement of the structural instability, called the global instability index (GII). The closer GII is to zero, the more stable is the structure. The pressure-induced local structural changes presented in Figs. 2(c) and 2(d) allow us to make the structural instability analysis. Figure S8 displays the BVS of the LiO_x cluster versus pressure together with the results at ambient pressure. The deviation of the BVS from 1 for the Li ion increases slightly to 8 GPa, but the deviation remains in the same range of the data at ambient pressure. At 10 GPa, the deviation jumps abruptly. We have calculated the BVS for the cluster LiO_9 (LB+SB) and LiO_3 (SB) separately in Fig. S8. A jump of BVS from 8 to 10 GPa is primarily due to the dramatic shortening of the SB at 10 GPa. At 12.66 GPa, although the x-ray diffraction pattern can be refined equally well with the $R\bar{3}c$ and the $R3c$ phases, the BVSs from these two structures are significantly different. At 12.66 GPa, whereas the deviation of the BVS from 1in the $R\bar{3}c$ phase is significantly high, the deviation in the $R3c$ phase is back in the range for the phases at ambient pressure. We can conclude that the $R3c$ phase is more stable at 12.66 GPa. The BVS remains close to 1 for $P > 12.66$ GPa.

The BVS analysis clearly reveals the local structural instability as the driving force for the Li displacement. One may still argue that the antiparallel displacement could be a solution for the global structure instead of the parallel displacement. BB have compared the $R3c$ and the $R\bar{3}$ with the antiparallel displacement. They can rationalize the greater stability of the $R3c$ phase versus the $R\bar{3}$ phase by the Pauling's third rule [6]. Xiang has also shown that the system energy is lowered to move Li into an octahedron to bond with three oxygens on the LB in the $R3c$ phase [7].

In conclusion, the polar phase can be stabilized at room temperature in metallic $LiOsO_3$ under 15.8 GPa. The driving force for the pressure-induced phase transition to the polar phase is solely the structural origin. Pressure creates a supercompacted LiO_3 triangle plane in the structure that makes the $R\bar{3}c$ phase unstable in terms of the bond valence of the Li bonding with oxygen. The Li displacement to form LiO_6 octahedra is a solution to optimize the local structure in order to reduce the BVS back to the formal valence of the Li ion. A weak electron-TO phonon interaction associated with the Li vibration is the consequence of the structural transition. This result offers a practical route to the design of different polar metals.

This work was supported by National Science Foundation Grants No. DMR-1905598 and No. DMR-1720595. K.Y. was supported in part by a research grant from Nippon Sheet Glass Foundation for Materials Science and Engineering (No. 40-37), and Innovative Science and Technology Initiative for Security (Grant No. JPJ004596), ATLA, Japan. J.F.L. acknowledges the support from Geophysics Program of the National Science Foundation Grant No. EAR-1916941. The authors are grateful to John B. Goodenough for commenting on the manuscript and V. Prakapenka for his assistance with the x-ray diffraction experiments at 13ID-D, GSECARS. GSECARS operations were supported by the National Science Foundation (EAR-1128799) and U.S. Department of Energy, Geosciences (DE-FG02-94ER14466)

[1] P. W. Anderson and E. I. Blount, Symmetry Considerations on Martensitic Transformations: "Ferroelectric" Metals? Phys. Rev. Lett. **14**, 217 (1965).

[2] Y. Shi, Y. Guo, X. Wang, A. J. Princep, D. Khalyavin, P. Manuel, Y. Michiue, A. Sato, K. Tsuda, S. Yu, M. Arai, Y. Shirako, M. Akaogi, N. Wang, K. Yamaura, and A. T. Boothroyd, A ferroelectric-like structural transition in a metal, Nat. Mater. **12**, 1024 (2013).

[3] N. J. Laurita, A. Ron, J. Y. Shan, D. Puggioni, N. Z. Koocher, K. Yamaura, Y. Shi, J. M. Rondinelli, and D. Hsieh, Evidence for the weakly coupled electron mechanism in an Anderson-Blount polar metal, Nat. Commun. **10**, 3217 (2019).

[4] D. Puggioni and J. M. Rondinelli, Designing a robustly metallic noncenstrosymmetric ruthenate oxide with large thermopower anisotropy, Nat. Commun. **5**, 3432 (2014).

[5] T. H. Kim, D. Puggioni, Y. Yuan, L. Xie, H. Zhou, N. Campbell, P. J. Ryan, Y. Choi, J.-W. Kim, J. R. Patzner, S. Ryu, J. P. Podkaminar, J. Irwin, Y. Ma, C. J. Fennie, M. S. Rzchowsi, X. Q. Pan, V. Gopalan, J. M. Rondinelli, and C. B. Eom, Polar metals by geometric design, Nature (London) **533**, 68 (2016).

[6] N. A. Benedek and T. Birol, "Ferroelectric" metals reexamined: Fundamental mechanisms and design considerations for new materials, J. Mater. Chem. C **4**, 4000 (2016).

[7] H. J. Xiang, Origin of polar distortion in $LiNbO_3$-type "ferroelectric" metals: Role of *A*-site instability and short-range interactions, Phys. Rev. B **90**, 094108 (2014).

[8] T. Gu, T. Scarbrough, Y. R. Yang, J. Iniguez, L. Bellaiche, and H. J. Xiang, Cooperative Couplings between Octahedral Rotations and Ferroelectricity in Perovskites and Related Materials, Phys. Rev. Lett. **120**, 197602 (2018).

[9] See Supplemental Material at http://link.aps.org/supplemental/10.1103/PhysRevB.101.220101 for detailed information on the experimental setup including Raman and x-ray diffraction with diamond anvil cells, the data analysis, parameters from Rietveld refinement of x-ray diffraction patterns, and the equation of state.

[10] F. Jin, A. Zhang, J. Ji, K. Liu, L. Wang, Y. Shi, Y. Tian, X. Ma, and Q. Zhang, Raman phonons in the ferroelectric-like metal $LiOsO_3$, Phys. Rev. B **93**, 064303 (2016).

[11] A. F. Goncharov, Raman spectroscopy at high pressures, Int. J. Spectrosc. (2012), doi: 10.1155/2012/617528.

[12] P. Postorino, A. Congeduti, E. Degiorgi, J. P. Itie, and P. Munsch, High-pressure behavior of $La_xSr_{2-x}MnO_4$layered manganites investigated by Raman spectroscopy and x-ray diffraction, Phys. Rev. B **65**, 224102 (2002).

[13] L. W. Finger, R. M. Hazen, G. Zou, H. K. Mao, and P. M. Bell, Structure and compression of crystalline argon and neon at high-pressure and room-temperature, Appl. Phys. Lett. **39**, 892 (1981).

[14] F. Jin, L. Wang, A. M. Zhang, J. T. Ji, Y. G. Shi, X. Q. Wang, R. Yu, J. D. Zhang, E. W. Plummer, and Q. M. Zhang, Raman interrogation of the ferroelectric phase transition in polar metal $LiOsO_3$, Proc. Natl. Acad. Sci. U.S.A. **116**, 20322 (2019).

[15] B. G. Hyde and M. O'Keeffe, Relations between $DO_9(ReO_3)$ structure type and some bronze and tunnel structures, Acta Crystallogr., Sect. A **29**, 243 (1973).

[16] R. H. Mitchell, *Perovskites, Modern and Ancient* (Almaz Press, Ontario, Canada, 2002).

[17] E. I. Paredes Aulestia, Y. W. Cheung, Y.-W. Fang, J.-F. He, K. Yamaura, K. T. Lai, S. K. Goh, and H.-H. Chen, Pressure-induced enhancement of non-polar to polar transition temperature in metallic $LiOsO_3$, Appl. Phys. Lett. **113**, 012902 (2018).